Drosophila Squid/hnRNP helps Dynein switch from a gurken mRNA transport motor to an ultrastructural static anchor in sponge bodies

Developmental Cell
Article

Drosophila Squid/hnRNP Helps Dynein Switch from a *gurken* mRNA Transport Motor to an Ultrastructural Static Anchor in Sponge Bodies

Renald Delanoue,[1,3,5] Bram Herpers,[2,3] Jan Soetaert,[1,6] Ilan Davis,[1,4,6,*] and Catherine Rabouille[2,4,*]
[1]Wellcome Trust Centre for Cell Biology, Michael Swann Building, University of Edinburgh, Mayfield Road, Edinburgh EH9 3JR, United Kingdom
[2]The Cell Microscopy Centre, Department of Cell Biology, Institute of Biomembranes, University Medical Centre Utrecht, Heidelberglaan 100, 3584 CX Utrecht, The Netherlands
[3]These authors contributed equally to this work and are listed in alphabetical order.
[4]These authors contributed equally to this work and are joint corresponding authors listed in alphabetical order.
[5]Present address: Centre de Biochimie, UMR CNRS 6543, Parc Valrose, Faculté des Sciences, 06108 Nice Cedex 2, France.
[6]Present address: Department of Biochemistry, Oxford University, South Parks Road, Oxford OX1 3QU, United Kingdom.
*Correspondence: ilan.davis@bioch.ox.ac.uk (I.D.), c.rabouille@umcutrecht.nl (C.R.)
DOI 10.1016/j.devcel.2007.08.022

SUMMARY

In *Drosophila* oocytes, dorso-anterior transport of *gurken* mRNA requires both the Dynein motor and the heterogeneous nuclear ribonucleoprotein (hnRNP) Squid. We show that *gurken* transcripts are transported directly on microtubules by Dynein in nonmembranous electron-dense transport particles that also contain Squid and the transport cofactors Egalitarian and Bicaudal-D. At its destination, *gurken* mRNA is statically anchored by Dynein within large electron-dense cytoplasmic structures known as sponge bodies. Egalitarian and Bicaudal-D contribute only to active transport, whereas Dynein and Squid are also required for *gurken* mRNA anchoring and the integrity of sponge bodies. Disrupting Dynein function disperses *gurken* mRNA homogeneously throughout the cytoplasm, whereas the loss of Squid function converts the sponge bodies into active transport particles. We propose that Dynein acts as a static structural component for the assembly of *gurken* mRNA transport and anchoring complexes, and that Squid is required for the dynamic conversion of transport particles to sponge bodies.

INTRODUCTION

mRNA localization directs the biosynthesis of proteins to specific subcellular compartments in all major model systems, including yeast, *Drosophila*, and a number of vertebrate models (St Johnston, 2005). mRNA localization occurs by several distinct mechanisms, including selective degradation (Bashirullah et al., 1999), diffusion followed by anchoring (Forrest and Gavis, 2003; Glotzer et al., 1997), and continual active transport (Weil et al., 2006), among other forms of delivery by molecular motors (Tekotte and Davis, 2002). The best-characterized case of a motor that transports RNA is Myosin V, which transports *Ash1* mRNA along actin microfilaments in yeast (Bertrand et al., 1998).

In the developing *Drosophila* oocyte, *gurken* (*grk*) mRNA encodes a secreted TGF-α signal and is localized at two different times in oogenesis, first posteriorly, then dorso-anteriorly. The Grk signal is targeted to the same locations, thus initiating the antero-posterior and dorso-ventral axes of the oocyte and future embryo (Neuman-Silberberg and Schüpbach, 1993; Gonzalez-Reyes et al., 1995; Pearson and Gonzalez-Reyes, 2004).

grk RNA is first transported from the nurse cells into the oocyte by the *Drosophila* Dynein motor (Clark et al., 2007; Caceres and Nilson, 2005), which is also required for transport to the oocyte dorso-anterior (MacDougall et al., 2003). The Dynein motor is a very large complex of many components, including the force-generating ATPase Dynein heavy chain and the Dynein intermediate and light chains (Pfister et al., 2006). The additional cofactors Bicaudal-D (BicD) and Egalitarian (Egl) are required in vivo for efficient Dynein-based mRNA transport, and are required in some way for the cargo to recruit the Dynein motor (Bullock and Ish-Horowicz, 2001; Bullock et al., 2006; Clark et al., 2007).

Although the evidence is good that Dynein is involved in the transport of various mRNAs in *Drosophila*, it is not known whether transport occurs by direct association of the mRNA cargo with Dynein or indirectly, by hitchhiking on a transport vesicle or along a membrane-bound compartment such as the endoplasmic reticulum (ER), as previously postulated for *Xenopus Vg1* (Deshler et al., 1997) and shown for *ASH1* (Schmid et al., 2006).

Once at its final destination, mRNA must be kept localized, a process that could occur by a number of possible mechanisms (Delanoue and Davis, 2005), including anchoring and continuous active transport. Actin-dependent tethering has been favored as a means of anchoring mRNA. However, F-actin is not required for anchoring of the apically localized *pair-rule* transcripts in blastoderm embryos. Instead, apical transcripts are tethered in a

microtubule- (MT) and Dynein-dependent manner, independently of the ATPase activity of the motor, BicD, and Egl, which are required for RNA transport (Delanoue and Davis, 2005). It is not currently known how *grk* mRNA is maintained at its final site of localization, nor whether any specialized structure or membrane-bound organelles are involved.

Some factors have been identified that are involved in *grk* mRNA localization (Roth and Schüpbach, 1994; Goodrich et al., 2004; Van Buskirk and Schüpbach, 2002), of which the best studied is Squid (Sqd), a *Drosophila* heterogeneous nuclear ribonucleoprotein (hnRNP) (Norvell et al., 1999). Like other hnRNPs, Squid probably binds to many RNAs in addition to *grk* in the oocyte and has many basic cellular functions. For instance, recently it was shown that Sqd is in a complex with Hrp48 and the *Drosophila* Imp protein, a complex required for *grk* and *osk* mRNA translation (Geng and MacDonald, 2006). However, the *Drosophila squid* null phenotype has a specific defect in the second step of *grk* mRNA transport rather than a more severe defect expected from an essential cellular factor (MacDougall et al., 2003; Norvell et al., 1999). It remains unclear whether Sqd is also required for RNA anchoring.

Here we address these questions by imaging and perturbing the movement and anchoring of *grk* RNA in living cells, in combination with immunoelectron microscopy (IEM) techniques we have developed to covisualize *grk* mRNA together with the components of the Dynein motor complex and its associated cofactors. We found that *grk* transcripts are transported to their final destination in nonmembrane-bound, nonmembrane transport particles directly associated with microtubules. At the dorso-anterior corner, *grk* transcripts are statically anchored in large cytoplasmic structures previously described as sponge bodies (Wilsch-Brauninger et al., 1997). We show that, as in the embryo, mRNA anchoring requires Dynein but not Egl and BicD (Delanoue and Davis, 2005), and that Dynein is required for the structural integrity of the anchoring complexes. We show that Squid is also necessary for *grk* RNA anchoring and for the efficient formation and maintenance of the sponge bodies. Our observations lead us to propose a model in which Sqd, Egl, BicD, and Dhc are all present in transport particles and sponge bodies but play distinct roles in the two steps of transport and subsequent anchoring. We further propose that Dynein is converted from an active motor acting on transport particles to a static component required for the structure of the sponge bodies and therefore for *grk* mRNA anchoring. In this model, Sqd is required in some way for the conversion of transport particles into sponge bodies and may therefore be involved in the conversion of Dynein from an active motor to a static anchor.

RESULTS

grk RNA Is Transported along MTs in Transport Particles Containing Dynein

The transport of *grk* RNA by Dynein could either be achieved by association with Dynein on MTs or indirectly by hitchhiking on another Dynein-dependent transport process, such as vesicular transport. To distinguish definitively between these possibilities, we used IEM methods on cryosections to codetect *grk* mRNA with MTs and Dynein motor components. We first studied the transport intermediates of injected biotinylated *grk* RNA in the center of early stage 9 oocytes. Twenty minutes after the injection, we fixed, recovered, and processed the egg chambers for IEM using methods we established for good membrane preservation of this tissue (Herpers and Rabouille, 2004). We found that injected *grk* RNA particles coassemble and concentrate in nonmembrane-bound electron-dense particles (Figures 1A–1C) that vary in size from 70 to 600 nm (Figures 1E and 1E′). In contrast, control injections of biotinylated *grk* RNA lacking the localization signal (*grkΔGLS*) do not assemble into transport particles and are diffusely localized in the cytoplasm (see Figure S1 in the Supplemental Data available with this article online). Although *grk* RNA transport particles are not consistently or specifically in close proximity to membrane-bound organelles, such as ER or vesicles, 67% of the observed particles are on, or within 100 nm from, the nearest MT. In comparison, only 33% of computer-generated randomly positioned particles of the same size are within the same distance from the nearest MT when placed on the same field of MTs. The difference in MT colocalization between *grk* RNA particles and randomly generated particles is statistically significant (Figures 1F and 1G).

We found that injected *grk* RNA colocalizes with the Dynein motor complex components Dhc and the motor cofactors Egl and BicD (Figures 1B, 1C, and 1I) in the transport particles. We estimate that there are likely to be many Dynein motors as well as RNA molecules in each electron-dense particle (quantified in Figures 1H and 1I). We conclude that injected *grk* RNA is transported directly on MTs by the Dynein motor in electron-dense RNP particles containing many *grk* RNA molecules and Dynein motor complexes, which we refer to as *grk* RNA "transport particles."

To investigate whether endogenous *grk* mRNA, like injected RNA, can be detected in transport particles, we developed methods of in situ hybridization on ultrathin cryosections followed by immunoelectron microscopy (ISH-IEM), allowing detection of the relatively low-abundance *grk* transcript (see Experimental Procedures). We identified endogenous transport particles as electron-dense small structures at the dorso-anterior corner that are labeled with usually one to three and sometimes more gold particles corresponding to *grk* mRNA (Figures 1D and 1H). These are smaller than the transport particles that assemble from injected *grk* RNA, although very similar in appearance and also closely associated with MTs (Figures 1F and 1G).

grk RNA Anchoring Is Static and Requires Intact MTs and Dynein, but Not Egl or BicD

To investigate whether the cytoskeleton plays a role in the retention of *grk* mRNA after transport to its final destination, we first covisualized the RNA with F-actin and MTs at the

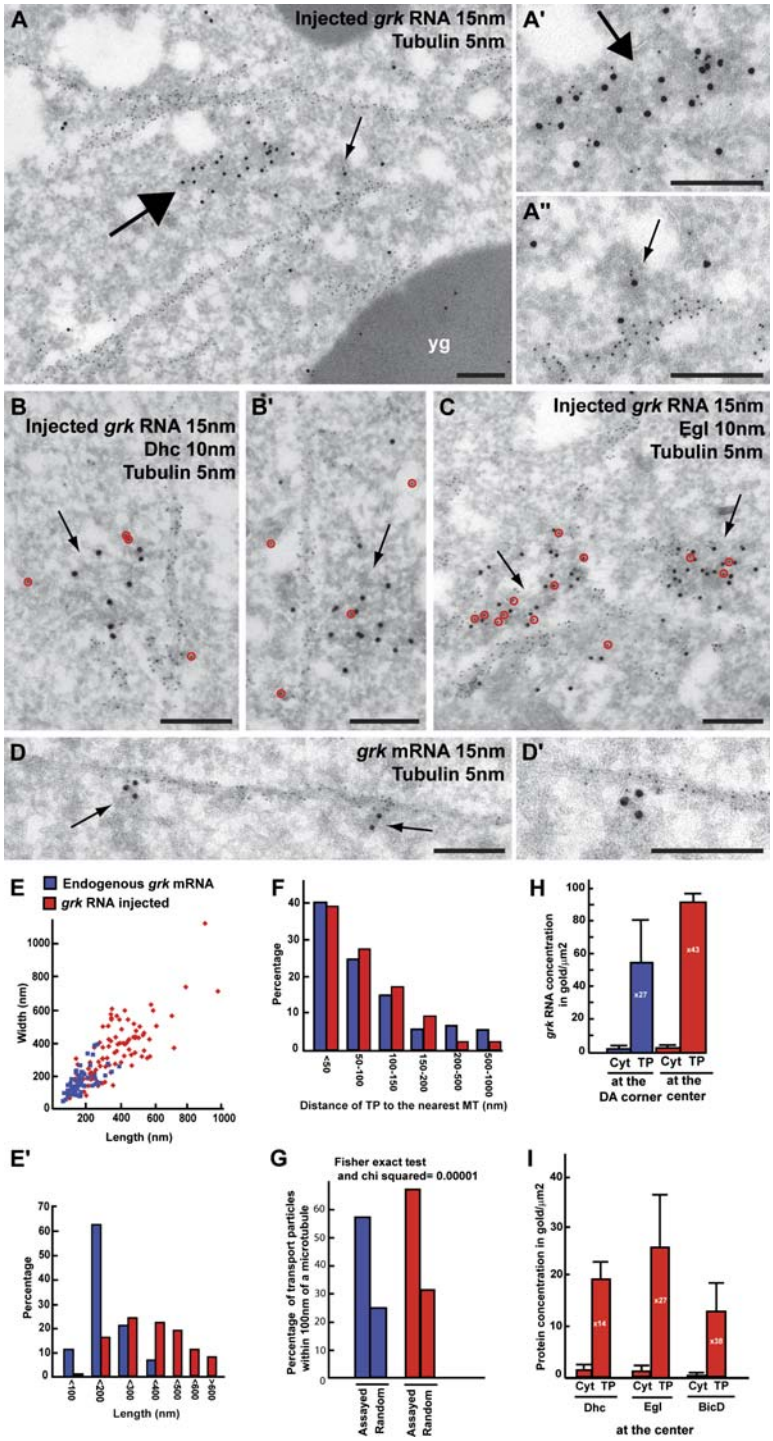

Figure 1. *grk* RNA Is Transported on MTs in Electron-Dense Nonmembrane-Bound Particles Containing Dynein

(A–A″) Wild-type oocyte injected with biotinylated *grk* RNA and fixed after 20 min. *grk* RNA (15 nm) is found in electron-dense transport particles ranging from 70 to 600 nm that are either on MTs (thin arrows) or near them (thick arrows). MTs are marked by α-tubulin (5 nm). yg, yolk granules.

(B and C) Transport particles labeled for *grk* RNA (15 nm), Dynein heavy chain (10 nm; red circles; [B and B′]), and Egl (10 nm, red circles; [C]) on MTs (5 nm).

(D and D′) Endogenous *grk* mRNA in stage 9 wild-type oocytes (15 nm) detected in transport particles associated with MTs (5 nm). In this and all subsequent figures, "*grk* mRNA" refers to the endogenous transcript and "*grk* RNA" to the injected RNA.

The scale bars represent 200 nm.

(E) Plot of the length versus width of transport particles.

(E′) Length distribution of the transport particle (nm).

(F) Distribution of the distance (nm) between a transport particle (TP) and the nearest MT.

(G) Quantification of the percentage of transport particles specifically associated with MTs (see the Supplemental Experimental Procedures).

(H) Density (in gold/μm^2) of endogenous (blue) and injected (red) *grk* RNA in transport particles (TP) compared to their surrounding cytoplasm (Cyt) (see the Supplemental Experimental Procedures). DA, dorso-anterior.

(I) Density (in gold/μm^2) of the Dynein complex components in transport particles formed upon injection of *grk* RNA (TP; red) compared to the surrounding cytoplasm (Cyt).

Error bars represent standard deviations.

site of localization by immunofluorescence. We found that *grk* RNA colocalizes with MTs (Figures 2A, 2C, and 2D) but not with F-actin (Figure S2A). We then inhibited F-actin polymerization with Latrunculin A and found that it had no effect on the localization of either endogenous or injected *grk* RNA (Figures S2B, S2C, S2E, and S2F). In contrast, depolymerizing MTs with Colcemid disrupts the localization of injected *grk* RNA (Figure 2D) and partly disrupts the localization of endogenous *grk* mRNA (Figure 2B). We conclude that MTs, but not F-actin, are required for the anchoring of *grk* mRNA at the dorso-anterior.

To test whether Dynein itself is required for this localization, we injected an inhibitory Dhc antibody into stage 9 oocytes 60 min after injection of *grk* RNA. We found that *grk* RNA anchoring is lost 3–5 min after injection of anti-Dhc antibody (Figure 2E). Similar results were obtained

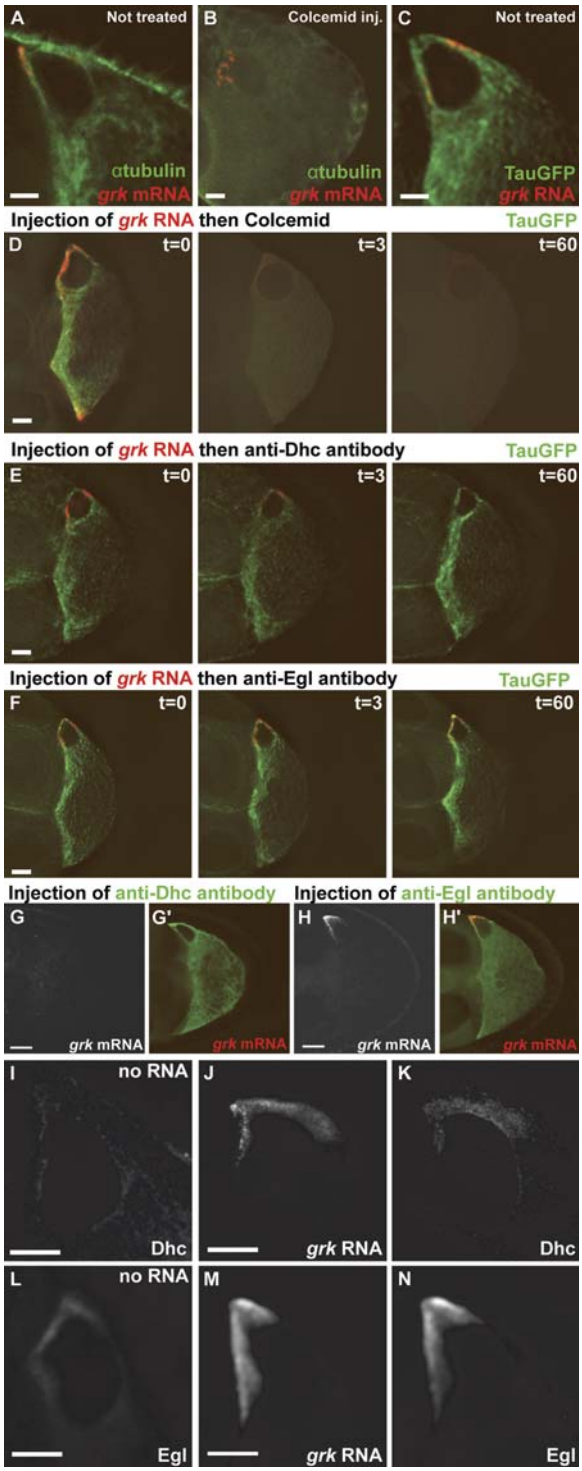

Figure 2. *grk* RNA Anchoring Depends on Intact MT and Dynein but Not Egl

(A) Endogenous *grk* mRNA in a stage 9 oocyte detected by FISH (red) colocalized with MTs (green).

(B) A stage 9 egg chamber treated for 45–60 min with Colcemid causing a severe, but incomplete, delocalization of endogenous *grk* mRNA detected by FISH (red). MTs (green) are depolymerized.

(C and D) Alexa Fluor 546-labeled *grk* RNA (red) 45 min after injection into a stage 9 oocyte expressing TauGFP (marking the MT network; green) colocalizes with MTs (C). It loses its localization upon Colcemid injection at t = 0. The anchoring of injected *grk* RNA at the cap is altered after a few minutes (t = 3 min), and at t = 60 min is no longer detected at the dorso-anterior corner (D).

(E) Alexa Fluor 546-labeled *grk* RNA (red) localized at the dorso-anterior corner in a stage 9 oocyte loses its localization upon anti-Dhc antibody injection at t = 0. At t = 60 min, no injected RNA is detected at the dorso-anterior corner.

(F) Alexa Fluor 546-labeled *grk* RNA (red) localized at the dorso-anterior corner in a stage 9 oocyte is unaffected upon anti-Egl antibody injection at t = 0. *grk* RNA anchoring at the cap remains at t = 60 min.

(G) Anchoring of endogenous *grk* mRNA (red) is disrupted by injection of anti-Dhc antibody, detected with anti-mouse Alexa Fluor 488 (green) (G′), 45–60 min after injection.

(H) Anchoring of endogenous *grk* mRNA (red) is not disrupted by injection of anti-Egl antibody, detected with anti-rabbit Alexa Fluor 488 (green) (H′), 45–60 min after injection.

(I–N) Dhc (I) and Egl (L) are slightly enriched at the dorso-anterior corner in an uninjected oocyte. Injection of Alexa Fluor 546-labeled *grk* RNA in a stage 9 oocyte leads to a large increase in detectable Dhc (K) and Egl (N), colocalized with *grk* RNA at the dorso-anterior corner (J and M).

The scale bars represent 10 μm.

with endogenous *grk* RNA (Figures 2G and 2G′). Control experiments showed that MTs are intact after the injection (Figure 2E), and injection of rabbit serum or IgG did not affect *grk* RNA anchoring (Figures S3D and S3E). In contrast, injection of anti-Egl antibodies did not lead to a loss of anchoring of either injected or endogenous *grk* RNA (Figures 2F and 2H), despite Egl being required for active Dynein motility and transport of *grk* RNA (Figures S3A and S3B). We conclude that the motor activity of Dynein is required for transport but not anchoring of *grk* mRNA.

The Dynein-dependent localization of *grk* mRNA at the dorso-anterior corner could represent a static anchoring by the Dynein motor by a similar mechanism as *pair-rule* transcripts in the blastoderm embryo (Delanoue and Davis, 2005). Alternatively, *grk* RNA could be continuously transported to the dorso-anterior by the Dynein motor, a model that predicts a continuous flow of RNA particles moving in and out the dorso-anterior area.

To distinguish between *grk* RNA static anchoring and continuous transport, we carried out fluorescence recovery after photobleaching (FRAP) experiments on fully localized injected *grk* RNA in wild-type egg chambers (i.e., 60 min after injection). We found that photobleached *grk* RNA that has completed only the first stage of transport and is temporarily localized at the anterior of the oocyte partially recovers (Figures 3A, 3C, and 3C′). The partial recovery followed by a slight drop in fluorescence is likely to be due to the fact that new unbleached RNA arriving in the anterior continues moving to the dorso-anterior. In contrast, photobleached localized *grk* RNA fails to recover at the dorso-anterior corner (Figures 3B, 3C, and 3C′). We conclude that *grk* RNA is not anchored at the anterior after completion of the first step of its localization, but is statically anchored once it arrives at the dorso-anterior corner.

An anchoring role for Dynein at the dorso-anterior corner predicts that the motor complex is recruited together with *grk* RNA to the site of anchoring. We tested this

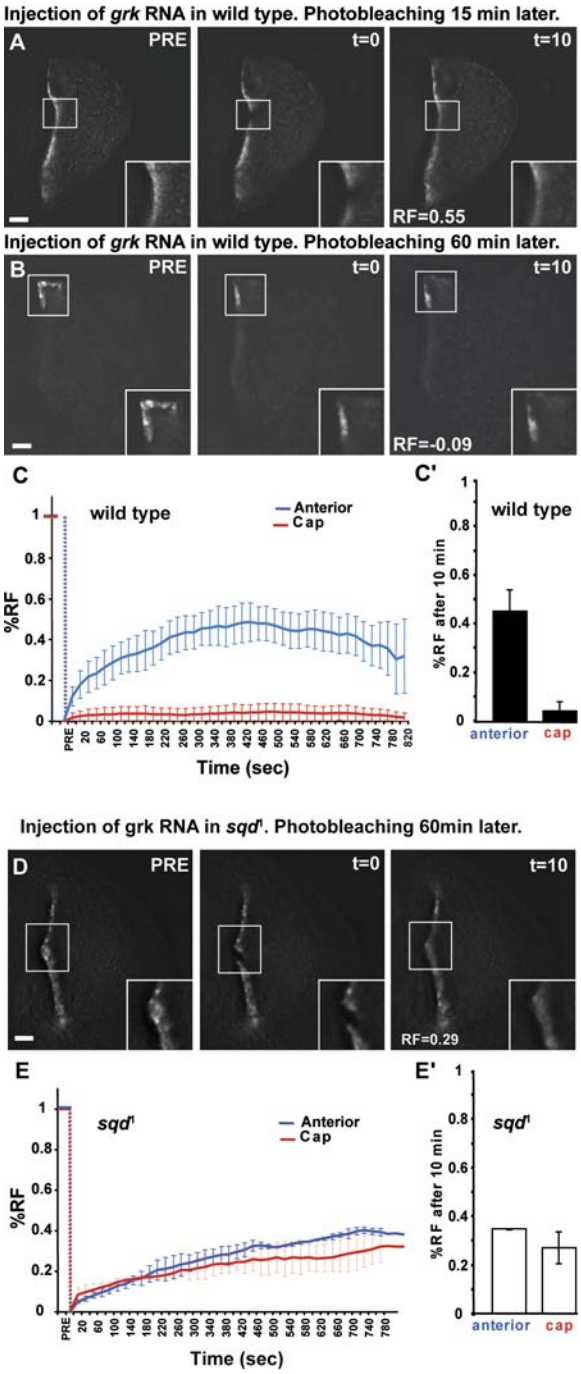

Figure 3. Injected *grk* RNA Is Statically Anchored at the Dorso-Anterior Corner in Wild-Type Oocyte but Not in *sqd*[1]

(A) A representative FRAP experiment in a living oocyte with Alexa Fluor 488-labeled *grk* RNA in midtransport (15 min after injection). At t = 0, a region of the anteriorly localized *grk* RNA is bleached (within the white square). A partial recovery of the signal is observed (recovery fraction, RF = 0.55) 10 min after bleaching (t = 10 min).

(B) A representative FRAP experiment of living oocyte showing Alexa Fluor 488-labeled *grk* RNA fully localized at the dorso-anterior corner (60 min after injection). At t = 0, a region of *grk* RNA is bleached (within the white square) and does not recover (RF = −0.09) 10 min later (t = 10 min).

(C) FRAP experiments in a wild-type living oocyte injected with Alexa Fluor 488-labeled *grk* RNA. The blue curve shows the recovery fraction (RF) at the anterior pole and the red curve shows the RF at the dorso-anterior corner. Averages and SD are made for each time point in at least three independent injected oocytes.

(C′) Percentage recovery of fluorescence 10 min after photobleaching in a wild-type oocyte. Bars represent the SD from at least three independent FRAP experiments.

(D) A representative FRAP experiment in a living *sqd*[1] mutant oocyte showing anterior localization of Alexa Fluor 488-labeled *grk* RNA (60 min after injection) immediately before photobleaching (PRE). Insets show higher magnifications of the bleached areas. The signal partly recovered 10 min after the bleaching (RF = 0.29).

(E) FRAP experiments in an *sqd*[1] living oocyte injected with Alexa Fluor 488-labeled *grk* RNA. The blue curve shows the recovery fraction (RF) at the anterior pole and the red curve shows the RF at the dorso-anterior corner. Averages and SD are made for each time point in at least three independent injected oocytes.

(E′) Percentage recovery of fluorescence 10 min after photobleaching in an *sqd*[1] oocyte. Bars represent the SD from at least three independent FRAP experiments.

Insets show higher magnifications of the bleached areas. The scale bars represent 10 μm.

prediction by visualizing components of the Dynein motor complex after injection of *grk* RNA and found that Dhc (Figures 2I–2K) and Egl (Figures 2L–2N) are both significantly enriched at the site of localization of the injected *grk* RNA, compared with uninjected controls (Figures 2I and 2L). Control injections of nonlocalizing *hunchback* (*hb*) RNA did not lead to any enrichment of Dynein motor components (Figures S3F–S3H). We conclude that Dynein is required for the static anchoring of *grk* mRNA at the dorso-anterior corner.

grk RNA Is Anchored at the Dorso-Anterior Corner in Sponge Bodies

pair-rule and *wingless* transcripts were previously shown to be statically anchored by Dynein in syncytial blastoderm embryos (Delanoue and Davis, 2005). It was hypothesized that apical mRNA anchoring occurs by the Dynein motor remaining attached to the cargo and MTs at the final destination. To test whether this hypothesis could apply to the static anchoring of *grk* mRNA in the oocyte, we used the ISH-IEM technique we developed (see above) to covisualize endogenous *grk* mRNA and the Dynein motor in stage 9 egg chambers. We found that at the dorso-anterior corner, endogenous *grk* mRNA is anchored together with the Dynein motor within large cytoplasmic structures whose ultrastructure is different in appearance from transport particles (Figures 4B–4D and 4G; see Figure S4 for an unadulterated version). Sectioning plastic-embedded wild-type oocytes revealed structures that are similar in appearance to previously described sponge bodies (Figure 4A; Wilsch-Brauninger et al., 1997) that were known to contain the protein Exuperantia (Exu) and to be found in nurse-cell cytoplasm. Although sponge bodies are present throughout the oocyte cytoplasm, the majority of *grk* mRNA is concentrated only in sponge bodies found at the dorso-anterior corner (Figures 4B–4D′). The minority of *grk* mRNA that is not in sponge bodies is found in the small transport particles we described (above) near or at the dorso-anterior corner and in the surrounding cytoplasm

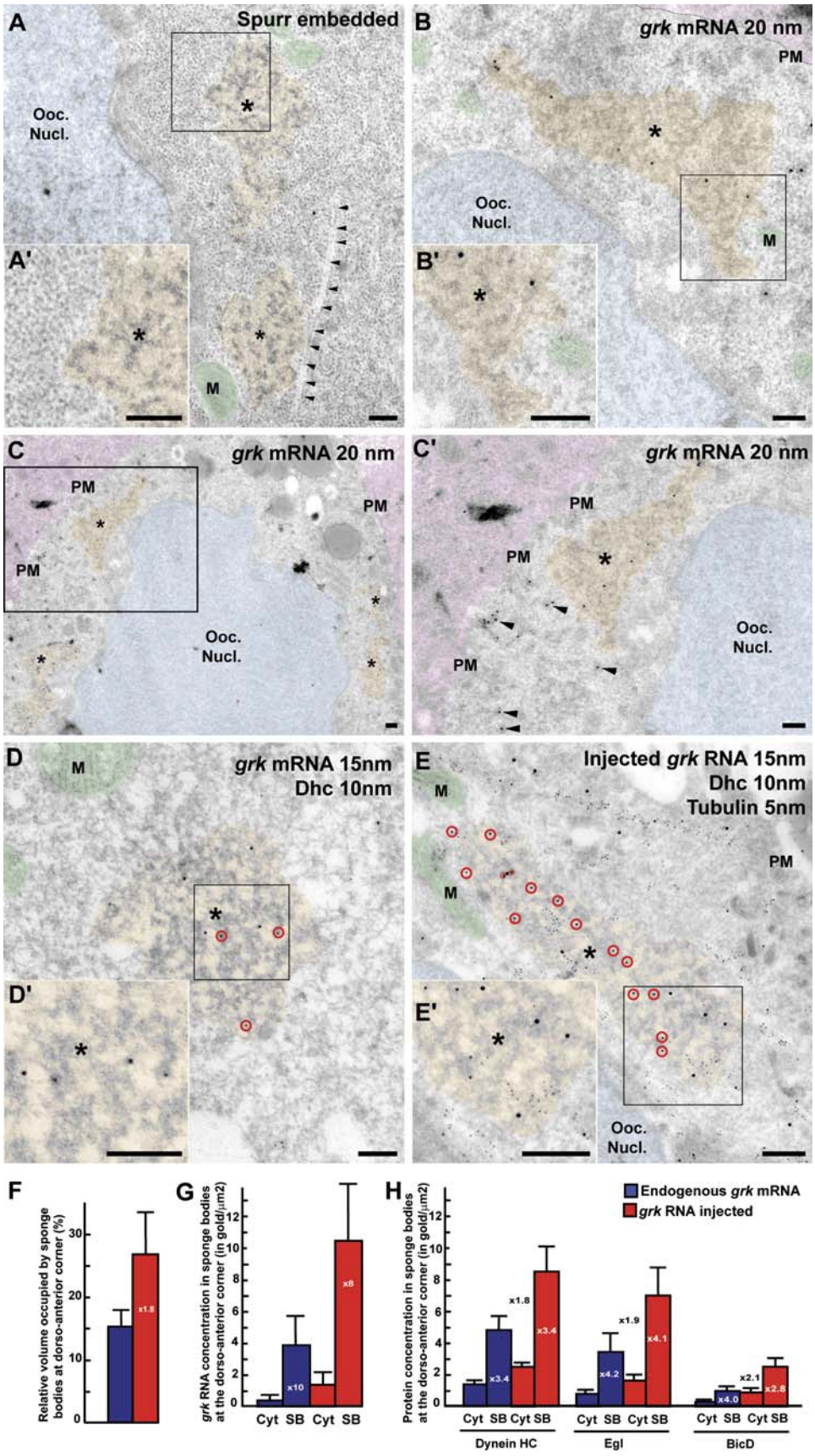
A
Spurr embedded
Ooc.
Nucl.
A'
M
B
grk mRNA 20 nm
PM
Ooc.
Nucl.
M
B'
C
grk mRNA 20 nm
PM
PM
PM
Ooc.
Nucl.
C'
grk mRNA 20 nm
PM
PM
PM
Ooc.
Nucl.
D
M
grk mRNA 15nm
Dhc 10nm
D'
E
Injected grk RNA 15nm
Dhc 10nm
Tubulin 5nm
M
M
PM
E'
Ooc.
Nucl.
F
Relative volume occupied by sponge bodies at dorso-anterior corner (%)
x1.8
G
grk RNA concentration in sponge bodies at the dorso-anterior corner (in gold/µm2)
x10
x8
Cyt SB Cyt SB
H
Endogenous grk mRNA
grk RNA injected
Protein concentration in sponge bodies at the dorso-anterior corner (in gold/µm2)
x1.8
x3.4
x3.4
x1.9
x4.1
x4.2
x2.1
x2.8
x4.0
Cyt SB Cyt SB
Dynein HC
Cyt SB Cyt SB
Egl
Cyt SB Cyt SB
BicD

(Figures 1 and 4C′). Sponge bodies are not membrane bound and can be as large as 2.5 μm. They consist of ''sponge-like'' electron-dense material, forming interconnected 60–90 nm wide strands that are interdigitated with cytoplasm and ER tubules. They are often flanked by MTs (Figure 4A) and, like transport particles, are enriched in Dhc, BicD, and Egl (Figures 4D and 4H; Figures S4F–S4H). Injected *grk* RNA is also enriched in sponge bodies at the dorso-anterior corner (Figures 4E and 4G) together with Dhc (Figures 4E and 4H), BicD, Egl (Figures S4G and S4H), and Hrp48 (data not shown). Remarkably, sponge body size and number are increased at the dorso-anterior corner by injecting *grk* RNA (Figure 4F). We conclude that Dynein-rich *grk* RNA transport particles are delivered to the dorso-anterior corner where the RNA is anchored in sponge bodies together with the Dynein motor complex and its cofactors.

Dhc Is Required for the Structural Integrity of Sponge Bodies

To investigate the function of Dynein in the anchoring of *grk* RNA in the sponge bodies, we studied the effect of inactivating Dynein function after anchoring of the RNA. We injected an inhibitory anti-Dhc antibody into stage 9 oocytes 60 min after injection of biotinylated *grk* RNA, as described in Figure 2E for the light microscopy assay, except that we then processed the samples for ultrastructural analysis. We found that disrupting Dhc function leads to a rapid redistribution of *grk* RNA into the cytoplasm (Figures 5A and 5B, arrows), in agreement with the results we obtained with fluorescence microscopy (Figure 2E). Surprisingly, we also found that the sponge bodies disappeared completely, and SqdGFP, which we used as a sponge body marker (see below), was also released into the cytoplasm (Figure 5B). In contrast, the inactivation of Egl, a cofactor for Dynein-dependent RNA motility, had no effect on sponge body integrity, as assessed by morphology and by the enrichment of SqdGFP in these structures (Figure 5C).

As Dynein has previously been suggested to play a role in MT organization (Vorobjev et al., 2001; Malikov et al., 2004), we tested whether the inactivation of Dynein causes an impairment of sponge body structure by affecting the MT cytoskeleton at the dorso-anterior corner, where it is most abundant. We found that MTs that normally flank the sponge bodies were unaffected by the injection of anti-Dhc antibodies (Figure 2E; Figures 5A and 5B, row of small arrowheads). We also found that depolymerization of MTs by Colcemid treatment did not affect sponge body integrity or the distribution of SqdGFP (Figure 5D).

To test this further, we used a hypomorphic combination of *dhc* alleles ($dhc^{6\text{-}6}/dhc^{6\text{-}12}$) that allows the study of developing oocytes. We found that sponge bodies are almost completely absent in *dhc* mutants (Figure 5F), compared with wild-type oocytes, where the sponge bodies are clearly visible (Figure 5E). We detected some small electron-dense structures, which we interpret either as remnants of sponge bodies or newly assembled transport particles (Figure 5F, arrowheads). In contrast to the *dhc* mutant, we found that sponge bodies are unaffected in *egl* and *BicD* mutant oocytes (Figures 5H–5J), despite most *grk* RNA transport being disrupted (Figure 5G). Some small amount of *grk* RNA does reach the dorso-anterior sponge bodies and is anchored in *egl* and *BicD*, and this increases when the RNA is injected near the dorso-anterior corner (Figures 5H–5J).

Considering all our results together, we conclude that Dynein is required for the structural integrity of the sponge

Figure 4. *grk* RNA Is Localized with Dynein in Dorso-Anterior Sponge Bodies

See Figure S4 for an unadulterated high-resolution version.

(A and A′) Sections of Spurr-embedded wild-type stage 9 oocytes showing large electron-dense sponge bodies (*) often flanked by MTs (row of small arrowheads) at the dorso-anterior corner. The square indicates the area shown at high magnification showing the difference in morphology between sponge bodies and the surrounding cytoplasm (A′).

(B) Endogenous *grk* mRNA is detected specifically at the dorso-anterior corner (20 nm) in sponge bodies (*). The squared area is shown at high magnification (B′) illustrating the similarity to the plastic section (A′) and showing the gold-labeled RNA. The thin line marks the oocyte plasma membrane (PM).

(C) Low-magnification view of the dorso-anterior corner of a stage 9 oocyte showing the endogenous *grk* mRNA both in sponge bodies (*) and in transport particles (arrowheads). The squared area is shown at high magnification (C′).

(D) Sponge bodies (*), where the endogenous *grk* mRNA (15 nm) is found, are also positive for Dhc (10 nm; red circles). The square indicates the area shown at high magnification (D′).

(E) Injected biotinylated *grk* RNA (15 nm) and Dhc (10 nm; red circles) also colocalize in sponge bodies (*) in a wild-type stage 9 oocyte, 60 min after injection. MTs are marked by α-tubulin (5 nm). The square indicates the area shown at high magnification (E′). For clarity, the oocyte nucleus (Ooc. Nucl.) is shaded in blue, the mitochondria (M) are in green, and the sponge bodies are in orange and marked by asterisks. Cells adjacent to the oocyte are colored in pink.

The scale bars represent 200 nm.

(F) Relative volume occupied by the sponge bodies at the dorso-anterior corner before and after *grk* RNA injection (see the Supplemental Experimental Procedures).

(G) Density (in gold/μm^2) of endogenous (blue) and injected *grk* RNA (red) in sponge bodies (SB) compared to their surrounding cytoplasm (Cyt) (see the Supplemental Experimental Procedures).

(H) Density (in gold/μm^2) of Dynein complex components in sponge bodies (SB) before (blue) and after (red) injection of *grk* RNA, compared with the surrounding cytoplasm (Cyt). Note that all the components are enriched about 3-fold in the sponge bodies (white numbers within bars), and that upon *grk* RNA injection, their concentration increases further (about 2-fold; black numbers next to bars). Taking into account that the volume of the sponge bodies is also increased by 1.8-fold, the concentration of these components increases about 4-fold at the dorso-anterior corner upon *grk* RNA injection.

Error bars represent standard deviations.

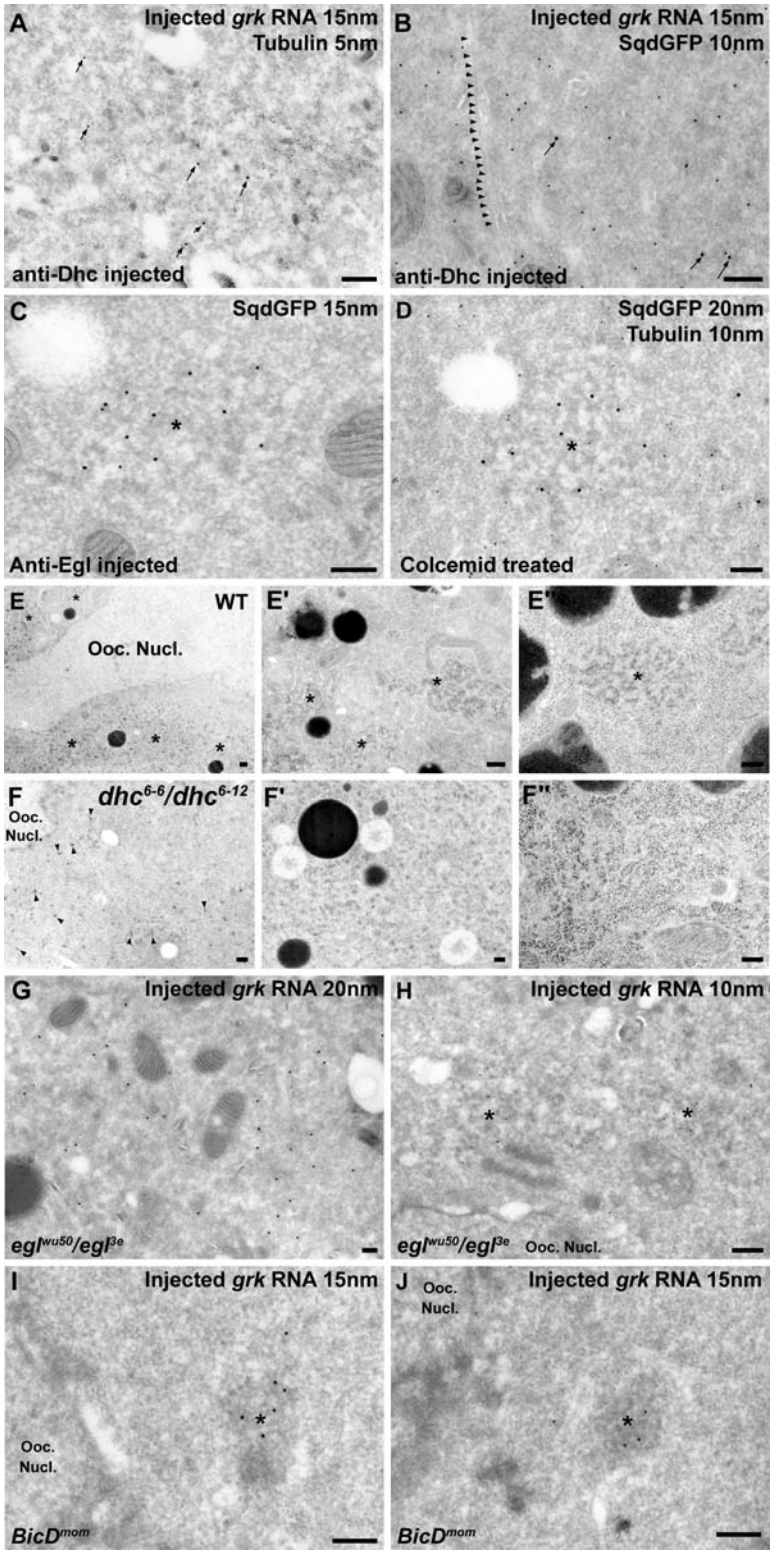

Figure 5. Dhc, but Not BicD and Egl, Is Required for the Structural Integrity of the Sponge Bodies

(A and B) Injected *grk* RNA (15 nm; arrows) and SqdGFP (10 nm; [B]) were found redistributed in the cytoplasm when SqdGFP-expressing ovaries with fully localized *grk* RNA were injected with anti-Dhc antibodies (as in Figure 2E) for 3, 5, or 10 min before fixation. Note that the sponge bodies containing *grk* RNA are no longer visible (compare to Figure 4E). Microtubules are marked with α-tubulin (5 nm; [A]) or by a row of small arrowheads (B).

(C) The inactivation of Egl by injection of anti-Egl antibody in SqdGFP oocytes does not affect sponge body structure, where SqdGFP (15 nm) remains concentrated.

(D) Colcemid treatment of SqdGFP oocytes leads to depolymerization of the microtubules (dispersed tubulin is detected with the anti-α-tubulin antibody; 10 nm) but does not affect the ultrastructure of the sponge bodies marked by SqdGFP (20 nm).

(E–E″) Three magnified images of Spurr-embedded wild-type oocytes showing that sponge bodies (*) are clearly visible around the oocyte nucleus (E) with their very characteristic structure (E′ and E″).

(F–F″) Three magnified images of Spurr-embedded *dynein* mutant oocytes showing that sponge bodies are no longer visible, and that the typical structure of electron-dense regions interdigitated with electron-light material is no longer observed. In (F), some small electron-dense structures (arrowheads) are present that could correspond to remnants of sponge bodies (*).

(G) Biotinylated *grk* RNA injected in the center of a stage 9 *egl* mutant oocyte fails to be transported to the dorso-anterior corner, does not form transport particles, and is not associated with the sponge bodies that are present.

(H) When *grk* RNA is injected at the dorso-anterior corner, it associates with the sponge bodies (*) at this location, showing that Egl is required for the transport but not the anchoring of *grk* RNA in sponge bodies.

(I and J) Biotinylated *grk* RNA injected at the dorso-anterior corner of a stage 9 $BicD^{mon}$ mutant oocyte, anchored in sponge bodies (*) at this location.

The scale bars represent 200 nm.

bodies in which it is concentrated. This function of Dynein does not require its RNA cargo transport activity, as it can occur in the absence of BicD and Egl, cofactors required for Dynein-based RNA motility in the embryo and oocyte.

Squid Is Also Enriched at the Dorso-Anterior Corner upon *grk* RNA Transport

The movement of *grk* mRNA to its site of anchoring has been previously shown to require two steps, the second

being Sqd dependent. To determine whether Sqd is present with *grk* RNA during and after completion of transport, we covisualized *grk* RNA and Sqd by IEM in SqdGFP-expressing egg chambers (Norvell et al., 2005). We found that SqdGFP colocalizes with injected *grk* RNA in the transport particles (Figures 6A and 6B). At the dorso-anterior corner SqdGFP is enriched in sponge bodies (Figures 6B and 6C), together with Dhc, BicD, and Egl (Figures 6E–6G). This raises the possibility that the enrichment of SqdGFP to the sponge bodies results from its association with the transported *grk* RNA. We tested this idea by injecting *grk* RNA and investigating whether this causes a further enrichment of SqdGFP at the same site. We found that injection of *grk* RNA into transgenic flies expressing SqdGFP leads to a strong enrichment of SqdGFP at the dorso-anterior corner (Figure 6H). We conclude that Sqd is at least partly recruited to the dorso-anterior corner through its association with *grk* mRNA.

In the Absence of Sqd, *grk* RNA Is Continuously Transported Rather Than Statically Anchored

To study in more detail the role of Sqd in *grk* mRNA localization, we studied *grk* RNA localization in *sqd* null mutant egg chambers. By injecting Colcemid or Latrunculin as in wild-type oocytes (Figure 2; Figure S2), we found that intact MTs, but not F-actin, are required for the anterior localization of injected and endogenous *grk* RNA in this mutant (Figures S5A–S5D). We then tested whether Dhc is required for the anterior localization of *grk* RNA in *sqd* mutant oocytes. The results show that the anterior localization of injected and endogenous *grk* RNA is disrupted by injection of anti-Dhc (Figures S5E and S5F) and anti-Egl (Figures S5G and S5H) but not by injection of control rabbit antiserum (Figures S5I and S5J). We conclude that in the absence of Sqd, *grk* mRNA localization at the anterior requires Dynein.

In a *sqd* mutant, Dynein could either be required for the static anchoring of the RNA at the anterior on MTs or to transport the RNA continuously at the anterior on MTs. To distinguish between these two possibilities, we carried out FRAP experiments. The results show that injected fluorescent *grk* RNA that accumulates at the anterior pole of *sqd* mutants recovers after photobleaching. The recovery was the same for the small pool of photobleached *grk* RNA localized at the dorso-anterior cap, albeit at a slightly slower rate. We conclude that in the absence of Sqd, *grk* RNA is in continuous flux at the anterior (Figures 3D, 3E, and 3E′).

Transport Particles Are Not Converted into Sponge Bodies in *sqd* Mutant Oocytes

Our results suggest that the localization at the anterior had different properties than the anchoring in sponge bodies at the dorso-anterior corner of wild-type oocytes. We used IEM to determine in which structures injected *grk* RNA is found in *sqd* mutant oocytes. We found that, despite the fact that uninjected *sqd* mutants have similar sponge bodies in shape and number to those in wild-type oocytes (Figures 7E and 7G), the vast majority of injected *grk* RNA was found in transport particles in *sqd* mutants (Figure 7A), even at the dorso-anterior corner. These transport particles also contain Dhc, BicD, and Egl (Figures 7B–7D), so in all aspects identical to wild-type transport particles. A very small proportion of *grk* RNA was also found in dorso-anterior corner sponge bodies (Figure 7F).

Taken together, our data demonstrate conclusively that *grk* transcripts are maintained at the anterior of *sqd* null mutant oocytes by continuous active transport using Dynein, rather than being statically anchored there. Therefore, Sqd is required for the movement of transport particles from the anterior to the dorso-anterior corner, raising the interesting possibility that Sqd could also be required for anchoring.

Sqd Is Required for Anchoring *grk* RNA at the Dorso-Anterior Corner

To test whether Sqd is required for the anchoring of *grk* RNA, we inactivated Sqd after *grk* RNA was fully anchored at the dorso-anterior corner. We first tried to inhibit Sqd function with two distinct anti-Sqd monoclonal antibodies, but these showed effect neither on the transport nor the anchoring of *grk* RNA. We interpret these results as indicating that these monoclonal antibodies, like many other cases, are not functionally inhibitory, as the antibody does not phenocopy the mutant phenotype. As an alternative approach, we used an Sqd protein trap line containing an intronic GFP insertion that produces an SqdGFP fusion protein acting as a fully functional replacement of the *sqd* gene (Norvell et al., 2005). We used western blots to demonstrate that the transgenic line only expressed SqdGFP fusion protein, and did not express any GFP or Sqd splice variants (Figure 8A).

We then injected an anti-GFP antibody to inactivate SqdGFP function in order to recapitulate an *sqd* mutant phenotype similar to the null allele. We found that injection of the anti-GFP antibody followed by injection of *grk* RNA leads to an accumulation of RNA at the anterior because of the disruption of the second step of *grk* RNA transport (Figure 8B). We conclude that the anti-GFP antibody disrupts SqdGFP function, thus leading to a phenotype indistinguishable from the *sqd* null allele.

To test the role of Sqd in anchoring, we allowed *grk* RNA to become fully localized for 60 min after its injection into the oocyte, at which time we injected the inactivating anti-GFP antibody. We found that within 20 min, injected *grk* RNA became detached from its site of anchoring in the dorso-anterior corner (Figure 8C) and was found completely delocalized after 50 min. To test whether Sqd is also required for the anchoring of endogenous *grk* mRNA, we injected anti-GFP antibody into SqdGFP egg chambers, and then processed them for in situ hybridization 15 min after the injection. The results show that the anchoring of endogenous *grk* mRNA is disrupted rapidly after inhibiting SqdGFP function (Figures 8D and 8D′). Control injections of anti-GFP antibody into wild-type oocytes, in which *grk* RNA was prelocalized, showed no effect on *grk* RNA anchoring (Figure 8E). Endogenous

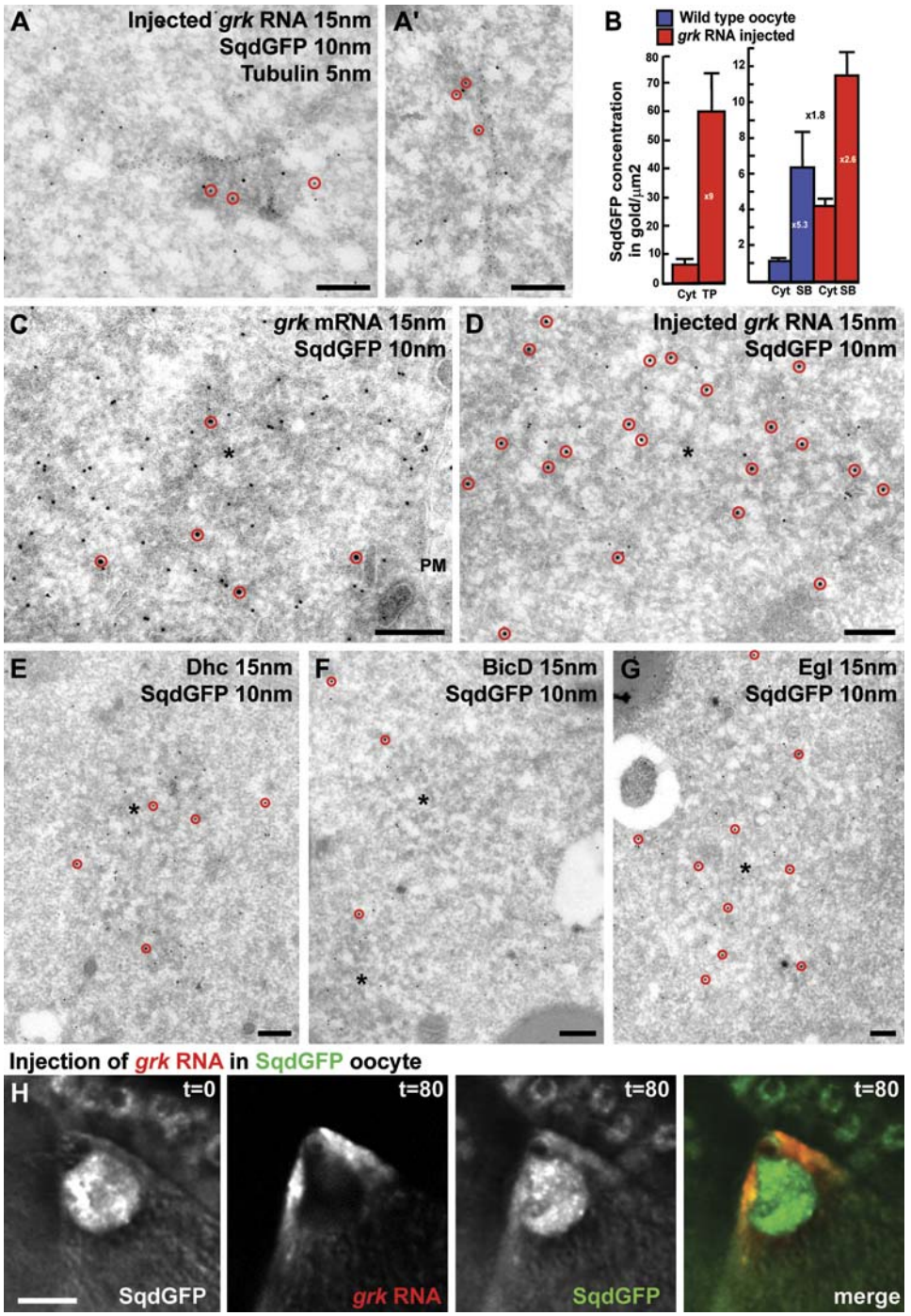

Figure 6. SqdGFP Colocalizes with *grk* RNA and the Components of the Dynein Motor Complex in Transport Particles and Sponge Bodies

(A and A′) Biotinylated *grk* RNA (15 nm) injected into a SqdGFP oocyte is found in transport particles on MTs (5 nm) together with SqdGFP (10 nm; red circles).

(B) Quantification of the concentration of SqdGFP in transport particles and sponge bodies when compared to the surrounding cytoplasm. Error bars represent standard deviations.

(C and D) SqdGFP (10 nm) colocalizes with endogenous *grk* mRNA (15 nm; red circles; [C]) and injected *grk* RNA (15 nm; red circles; [D]) in sponge bodies (*) at the dorso-anterior corner.

(E–G) SqdGFP (10 nm) colocalizes with Dhc (15 nm; red circles; [E]), BicD (15 nm; red circles; [F]), and Egl (15 nm; red circles; [G]) in sponge bodies (*).

(H) SqdGFP becomes enriched at the dorso-anterior corner upon injection of Alexa Fluor 546-labeled *grk* RNA in a stage 9 oocyte. At t = 0, SqdGFP is mostly in the nucleus. At t = 80 min, SqdGFP is enriched at the dorso-anterior corner with *grk* RNA (merge).

The scale bars represent 200 nm, except in (H), where the scale bar represents 10 µm.

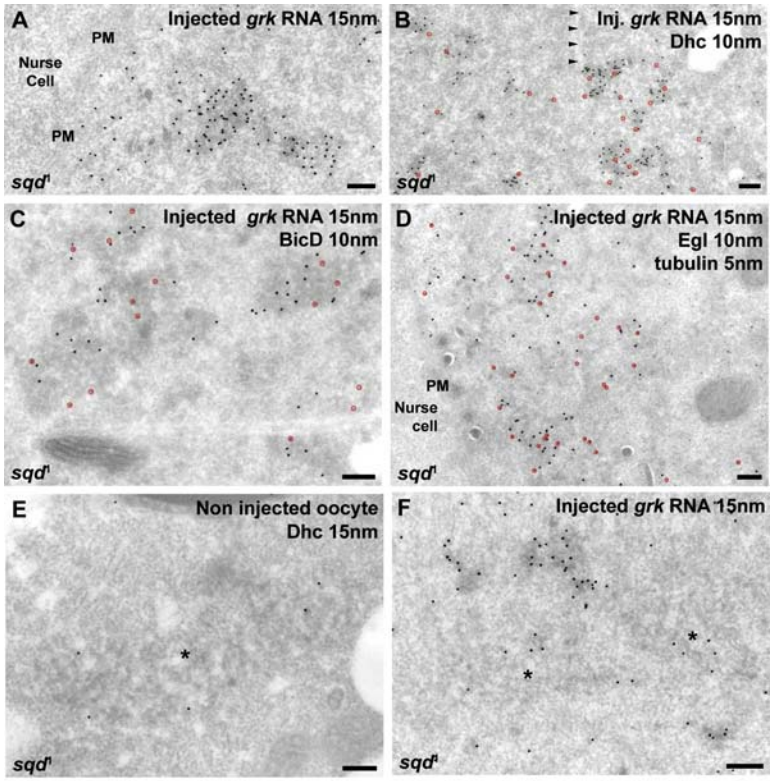

G	% of injected *grk* RNA in SB at the DA corner	volume of cytoplasm occupied by SB at the DA corner		% of injected *grk* RNA in TP along the anterior	density of injected *grk* RNA in TP (gold/μm2)
		before injection	after injection		
Wild type	75±5	15±3	27±6	0	
*sqd*1	1.5±0.2	11±2	0.5±0.5	76.6±6.4	120±35

Figure 7. Injected *grk* RNA Is Found in Transport Particles in *sqd*[1]

(A and B) In the *sqd*[1] mutant, biotinylated injected *grk* RNA (15 nm) is found at the anterior side (within 5 μm of the anterior plasma membrane) in transport particles along MTs (row of small arrowheads) that contain Dhc (10 nm; [B]). Red circles in (B) indicate Dhc that is present in transport particles.

(C and D) The transport particles described in (A) also contain BicD ([C]; 10 nm; red circles) and Egl ([D]; 10 nm; red circles) along MTs (5 nm).

(E) In a uninjected *sqd*[1] mutant oocyte, sponge bodies are also present and contain Dhc (15 nm).

(F) *sqd*[1] mutant oocyte injected with biotinylated *grk* RNA. The RNA is mostly found in transport particles but a very small amount is also found in one of the rare sponge bodies (*) that are still present after injection (see [G]). The scale bars represent 200 nm.

(G) Quantification of the conversion of sponge bodies into transport particles upon *grk* RNA injection in *sqd*[1]. Note that the sponge bodies that are present before injection (see Figure 7E) are almost absent 20 min after injection of *grk* RNA, which is found in transport particles along the anterior at a density similar to the transport particles found in the middle of wild-type injected oocytes (see Figure 1A). ± represents standard deviations.

grk mRNA in wild-type oocytes was also completely unaffected by the injection of anti-GFP antibody (Figure 8F). Finally, control injections of anti-GFP antibody into ubiquitously expressing nlsGFP or GFP transgenic lines did not have any effect on the localization of injected *grk* RNA (data not shown). We conclude that Sqd is required for anchoring both injected and endogenous *grk* mRNA at the dorso-anterior corner.

Inhibition of Dynein after anchoring of mRNA leads to the disappearance of the sponge bodies and transport particles, and to *grk* RNA being distributed throughout the cytoplasm (Figure 5). To determine whether the role of Sqd in anchoring is through being required for the structural integrity of sponge bodies, we analyzed where *grk* RNA is found after inactivation of SqdGFP. Ultrastructural analysis revealed that, when SqdGFP function is inhibited, injected *grk* RNA is found in transport particles rather than in sponge bodies (Figure 8G). These transport particles are indistinguishable from anterior *grk* RNA transport particles in *sqd* null mutants (Figure 7), suggesting that disrupting Sqd function converts sponge bodies into transport particles. Endogenous *grk* mRNA was also found in particles resembling endogenous transport particles near MTs (Figure 8H) that also contain Dynein (Figure 8I). We conclude that whereas Sqd is not required for transport particle integrity, it is essential for anchoring *grk* RNA at the dorso-anterior corner by maintaining the transcript in sponge bodies rather than in transport particles. Therefore, the role of Sqd in anchoring is distinct from that of Dhc. We propose that Sqd is required for the conversion of transport particles into sponge bodies, rather than the ability of transport particles to move. In contrast, Dhc is required for both the motility of the transport particles and for *grk* mRNA anchoring through a role in the integrity of the sponge bodies.

DISCUSSION

We have analyzed the molecular mechanism of *grk* mRNA transport and anchoring in the *Drosophila* oocyte using a number of novel methods, combining live cell imaging of oocytes with immunoelectron microscopy to covisualize *grk* RNA and transacting factors. We show that *grk* mRNA is transported in particles containing many individual RNA molecules assembled with numerous molecules of Dynein motor components and Squid. Approximately

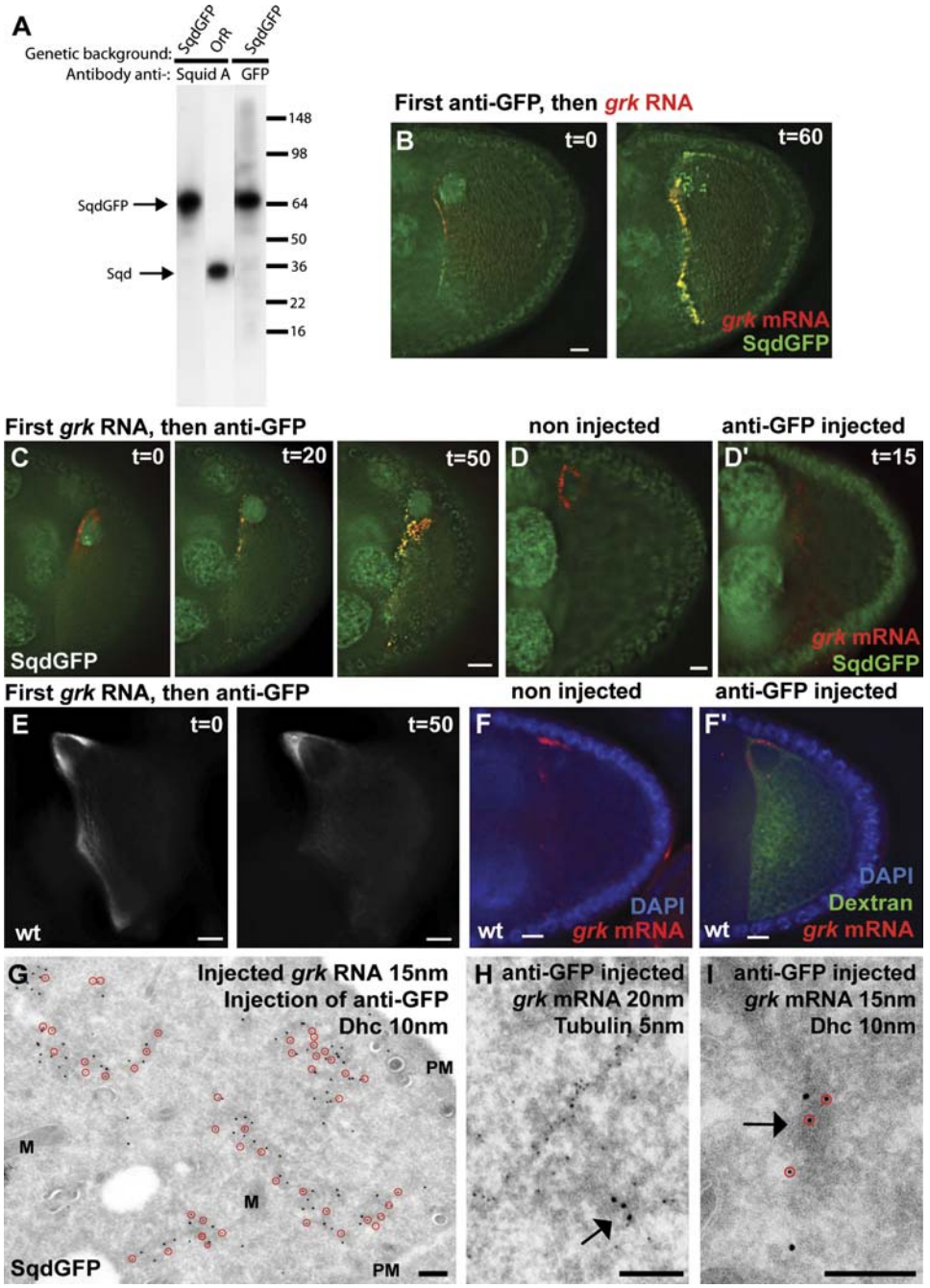

Figure 8. Sqd Is Involved in *grk* RNA Anchoring at the Dorso-Anterior Corner

(A) Western blot visualizing SqdA and SqdGFP in wild-type and SqdGFP oocytes, showing that neither GFP nor Sqd is expressed as a splice variant in SqdGFP.

(B) SqdGFP oocyte injected first with anti-GFP antibody followed by Alexa Fluor 546-labeled *grk* RNA at t = 0. *grk* RNA fails to reach the dorso-anterior corner and localizes at the anterior after 60 min (similar to *sqd*[1] mutant).

(C) SqdGFP oocyte injected with Alexa Fluor 546-labeled *grk* RNA, which became fully anchored after 60 min. anti-GFP antibody was then injected (t = 0), leading to the loss of *grk* RNA anchoring after 20 min.

(D and D′) Anchoring of endogenous *grk* mRNA (red) is disrupted by injection of anti-GFP antibody in an SqdGFP oocyte, 15 min after injection (D′). *grk* mRNA anchoring at the dorso-anterior corner is lost and the RNA is found along the anterior side.

(E) Wild-type oocyte injected with Alexa Fluor 546-labeled *grk* RNA, which became anchored. Injection of the anti-GFP antibody at t = 0 has no effect on the dorso-anterior corner localization of *grk* RNA.

(F) Anchoring of endogenous *grk* mRNA (red; detected by FISH) is not disrupted by injection of the anti-GFP antibody mixed with lysine-fluorescein-dextran (green; [F′]) in a wild-type oocyte.

two thirds of transport particles are in close association with MTs and are not consistently associated with membranes, such as ER or vesicles. This supports the idea that *grk* RNA particles are transported directly by motors on MTs. This notion is strengthened by the fact that the directed movement of the transport particles is disrupted very rapidly when MTs are depolymerized and Dhc, BicD, or Egl function is inhibited (MacDougall et al., 2003). Furthermore, the particles we observe moving along MTs in live cell imaging experiments correspond well to the similar-sized *grk* RNA-rich particles that we visualize by EM. The direct movement of *grk* RNA particles along MTs is in stark contrast to the transport of yeast *ASH1* RNA, which is thought to be cotransported with ER membrane (Schmid et al., 2006).

Once delivered to its final destination at the oocyte dorso-anterior corner, many copies of both injected *grk* RNA and endogenous *grk* mRNA are anchored in large electron-dense structures previously described as sponge bodies, together with the same components present in the transport particles, including Dynein and Squid. Sponge bodies are distinct in appearance from transport particles and have been previously described in nurse cells (Wilsch-Brauninger et al., 1997) and hypothesized to be RNA transport intermediates from the nurse cells to the oocyte. Although we have found Exu-GFP in *grk* anchoring structures (data not shown), we have identified them in the oocyte as functioning in anchoring, rather than transport, and containing components of the Dynein complex Dhc, Egl, and BicD. These data show that the endoplasmic reticulum is not involved in the transport and anchoring of *grk* mRNA, contrary to a previous proposal (Saunders and Cohen, 1999).

Transport particles and sponge bodies are related to RNA particles (also termed germinal granules, P bodies, and neuronal granules; St Johnston, 2005; Anderson and Kedersha, 2006) that display a large spectrum of sizes, composition, and morphology, reflecting several functions in RNA transport, storage, translational control, and processing. Nevertheless, it seems likely that the transport particles we have identified are related to *bcd* and *osk* mRNA granules (Chekulaeva et al., 2006; Tekotte and Davis, 2006) as well as to neuronal RNA granules (St Johnston, 2005). Our data demonstrate that sponge bodies play key roles in RNA anchoring, but it is not known whether they are also involved in translational control, degradation, and storage of mRNA.

Dynein is not only present in the sponge bodies but is also required for the static anchoring of *grk* RNA in the sponge bodies. However, anchoring does not require Egl or BicD, the motor cofactors that are required for RNA transport in the embryo and oocyte (this work; Bullock and Ish-Horowicz, 2001; Delanoue and Davis, 2005; Bullock et al., 2006; Navarro et al., 2004; Clark et al., 2007). While it is not certain whether Egl and BicD are required for cargo loading, transport initiation, or motor activity itself, our evidence shows that none of these functions are required for anchoring. *grk* RNA is therefore anchored by a similar mechanism to *pair-rule* and *wingless* transcripts in the syncytial blastoderm embryo. In both the embryo and oocyte, we propose that when the Dynein motor complex reaches its final destination, the motor becomes a static anchor that no longer depends on the transport activity of the motor.

Dynein (but not Egl and BicD) is not only a static anchor but is also required for the structural integrity of the *grk* RNA anchoring structures in the oocyte, the sponge bodies. Their rapid speed of disassembly upon Dynein inhibition (3–5 min) argues that Dynein has a direct role in anchoring and is required to form and maintain the large RNP complexes that constitute the sponge bodies. This evidence rules out that Dynein could indirectly be required for the delivery of anchoring components that are then used in anchoring *grk* when it is delivered to the sponge bodies. Dynein could also tether the cargo complex directly on the MTs when the transport particles reach their final destination, but our results show that MTs only flank the sponge bodies and are not, as predicted by this model, consistently interdigitated with most of the cargo and motor molecules we detect in the sponge bodies. This is also consistent with the fact that disassembling MTs does not lead to a change in sponge body structure and only leads to a partial loss of endogenous *grk* mRNA anchoring.

In addition to its previously documented role in the second step of *grk* mRNA transport, we have identified here a novel function for hnRNP Squid that plays an essential role in the anchoring of *grk* RNA at the dorso-anterior corner. Like Dynein, Sqd is also enriched at the site of anchoring upon injection of excess *grk* RNA. Inactivation of Sqd before transport begins leads to *grk* transport particles being present at the anterior of the oocyte in permanent anterior flux without anchoring, even for the particles that reach the dorso-anterior corner. Conversely, inactivation of Sqd after *grk* RNA arrives at the dorso-anterior corner leads to a breakdown of anchoring and the conversion of sponge bodies into anterior transport particles containing *grk* RNA. This suggests an active role for Sqd in keeping anchoring structures intact, and most likely a role for Sqd in promoting the conversion of transport particles into anchoring structures by facilitating their reorganization into anchoring complexes.

We propose that sponge bodies are assembled at the dorso-anterior corner by delivery of *grk* mRNA, Dynein

(G) Same experiment as described in (C) but with biotinylated *grk* RNA. After processing this sample for IEM, *grk* RNA (15 nm) was found along the anterior side in particles positive for Dhc (10 nm; red circles) and with the exact same features as the transport particles.
(H and I) SqdGFP oocytes injected with anti-GFP antibody (as in [D′]) were processed for ISH-IEM to detect endogenous *grk* mRNA (15 nm) that was found along the anterior side and partly in particles (arrows) positive for Dhc (10 nm; red circles; [I]) and next to microtubules (H). M, mitochondria; P, plasma membrane.
The scale bars represent 10 μm for (B)–(F) and 200 nm for (G)–(I).

motor component and Squid present together in transport particles. First, the same components are present in the transport particles and in the sponge bodies. Second, some transport particles containing endogenous *grk* mRNA are detected on dorso-anterior MTs. Third, injection of a large excess of *grk* RNA leads to an increase in the size and number of sponge bodies.

At the dorso-anterior corner, sponge bodies are maintained by both Dynein and Squid. When the Dynein motor complex reaches its final destination, the motor becomes a static anchor that no longer depends on the transport activity of the motor. Given the size of Dhc and the presence of many putative domains whose function remains elusive but that could play a central role in the switch from motor to anchor, we propose that it can associate with many other cellular factors to form a large and immobile anchoring complex. Sqd is known to be involved in translational regulation (Norvell et al., 2005), and we propose that association with this class of factors could help create a large and immobile anchoring complex. A strong link between molecular motors and hnRNPs has already been shown to control the localization of their associated mRNAs. For instance, She2 hnRNP acts as a linker between the Myosin motor complex and its mRNA cargo (Kruse et al., 2002). Kinesin and hnRNP are present together in RNA-transporting granules in neurons (Kanai et al., 2004). We propose that transport and anchoring of mRNA by molecular motors involve assembly into transport particles followed by reconfiguration of the same components into large electron-dense anchoring complexes at the final destination. Future work will establish how widely this model can be applied. It will also be interesting to determine whether the specificity of transport and anchoring of other RNA cargos in the *Drosophila* oocyte and embryo is also established by distinct combinations of RNA-binding proteins that influence the function of molecular motors. Time will tell what proportion of mRNA is anchored like *pair-rule* and *grk* transcripts by static functions of molecular motors, as opposed to other possible mechanisms of anchoring.

EXPERIMENTAL PROCEDURES

Fly Strains

Stocks were raised on standard cornmeal-agar medium at 25°C or 21°C. Wild-type was Oregon R (OrR); or SqdGFP (A. Debec); nuclear marker: four copies of the *nlsGFP* transgene (*yw; nlsGFPM; nlsGFPN*) (Davis et al., 1995); MT marker: TauGFP (D. St Johnston). Egl^{wu50}/Egl^{3e} (R. Lehmann) and $BicD^{mom}$ (B. Suter) flies were *w; Df(2L)TW119/* $BicD^{r8}$*; P [w+hsBic-D]-94/+* (Swan and Suter, 1996). *sqd* mutant alleles used were sqd^{1} (T. Schüpbach).

Injection of RNA and Inhibitors

RNA was transcribed in vitro using T7, T3, or SP6 polymerase with UTP-Alexa Fluor 546, UTP-Alexa Fluor 488, or UTP-biotin (Wilkie and Davis, 2001). We used the full-length *grk* cDNA, as smaller fragments are difficult to detect in EM. Ovaries were dissected and separated into individual ovarioles directly onto coverslips in series 95 halocarbon oil (KMZ Chemicals) and injected with labeled *grk* RNA using Femtotip needles (Eppendorf). RNA was injected at a concentration of 250–500 ng/μl, Colcemid (Sigma) at 1 mg/ml, and Latrunculin A (Sigma) at 20 mM. Anti-Dhc (D. Sharp), anti-Egl (R. Lehmann), anti-GFP (ascites from Sigma G6539, containing 25 mg/ml total protein, 5.8 mg/ml IgG), anti-Sqd (T. Schüpbach), and IgG and rabbit serum were injected at the same concentration (20 mg/ml). Each experiment was repeated with at least two different batches of RNA in a total of at least 12 and on average 25 egg chambers (Table S1). Egg chambers injected with anti-GFP antibody and 70 kDa lysine-fluorescein-dextran (Molecular Probes; injected at 0.125 mg/ml) were fixed and processed for endogenous *grk* mRNA in situ hybridization, with the uninjected controls in the same tube.

Antibodies

To detect the biotinylated RNA, we used Alexa Fluor 546-coupled avidin (Molecular Probes) or a polyclonal rabbit anti-biotin (Rockland) at 1:10,000 for IEM. We used anti-α-tubulin-FITC (Sigma; 1:1,000), monoclonal anti-α-tubulin B512 (Sigma) at 1:5,000 for IEM; rabbit polyclonal anti-Dhc, PEP1 (T. Hays) at 1:100 and 1:300 for IEM; rabbit polyclonal anti-Egl (R. Lehmann) at 1:4,000 and 1:300 for IEM; monoclonal anti-BicD 1B11 (B. Suter) at 1:20; and clones 2G10 and 4C2 at 1:20 for IEM; rabbit polyclonal anti-GFP A6455 (Molecular Probes) at 1:300 and FITC-phalloidin to label F-actin. For IEM, rabbit polyconal antibodies were detected directly with protein A gold conjugates (Department of Cell Biology, Institute of Biomembranes, Utrecht, The Netherlands). Mouse monoclonals were detected with rabbit anti-mouse (Dako; 1:250) followed by protein A gold conjugates. Anti-SqdA 2G9 (T. Schüpbach) was used at 1:1,000 for western blots.

Immunofluorescence and RNA Fluorescence In Situ Hybridization

Injected oocytes were fixed for 20 min or 1 hr in 4% paraformaldehyde (PFA; Polysciences) added directly on top of the egg chambers in halocarbon oil. Fixed oocytes were then recovered with glass pipettes into glass multiwell plates, and fixative and oil were washed away with PBS. Postfixation was performed with 4% PFA for 20 min, followed by several washes with PBT (PBS + 0.1% Tween). After fixation, ovaries were immunolabeled and processed for fluorescence in situ hybridization (FISH) as described previously (Wilkie et al., 1999) using fluorescent tyramide detection (NEN Life Sciences) and mounted in Vectashield (Vector). The digoxigenin-labeled antisense probes were prepared from a full-length *grk* cDNA (T. Schüpbach).

Four-Dimensional Imaging and Deconvolution

Imaging was performed on a wide-field DeltaVision microscope (Applied Precision, Olympus IX70 and with a Roper Coolsnap HQ, based on an original design by D.A. Agard and J.W. Sedat) with 20×/0.75 NA or 100×/1.4 NA objectives and then deconvolved using SoftWorks (Applied Precision) based on Sedat/Agard algorithms (Parton and Davis, 2006). Up to 25 egg chambers were imaged in parallel (Parton and Davis, 2005). Photobleaching experiments used a 488 nm laser with one iteration at the maximum intensity and measurement of the recovery of the fluorescence initiated 1 s later. Images were analyzed using SoftWorks (Applied Precision).

Sample Preparation for EM Analysis

Oocytes were embedded in Spurr as previously described (Herpers and Rabouille, 2004). Images were captured on a Jeol EX1200 electron microscope.

Detection of Injected *grk* RNA by Immunoelectron Microscopy

Egg chambers were injected in series 95 halocarbon oil and left for either 20 min for transport studies or 45–60 min for anchoring studies. Fixation was performed for a minimum of 3 hr using 2% electron-grade PFA and 0.2% glutaraldehyde (GA; Sigma) in 0.1 M phosphate buffer (pH 7.4), before being transferred and stored in 1% PFA in the same buffer at 4°C. Single stage 9 oocytes were embedded in blocks of 12% gelatin that were infused in 2.3 M sucrose and frozen in liquid

nitrogen. Sixty nanometer ultrathin sections were cut and collected on carbon-coated formvar copper grids as previously described (Herpers and Rabouille, 2004). The injected RNA was detected using polyclonal rabbit anti-biotin antibodies followed by protein A gold conjugates.

grk mRNA ISH-IEM

Egg chambers were fixed overnight in 4% PFA or 3 hr in 2% PFA, 0.2% GA in 0.1 M phosphate buffer (pH 7.4). Sixty nanometer sections were retrieved on carbon-coated formvar nickel grids on a drop of sucrose/methylcellulose mixture that was washed off by floating the grids three times for 5 min on drops of PBS at 37°C. The sections were postfixed in 1% GA in PBS and washed another three times in PBS. Prehybridization was performed at 37°C in 50% formamide (Sigma), 2× SSC in diethylpyrocarbonate-treated H_2O for 15 min. Biotinylated *grk* RNA probes were made according to the manufacturer's specifications (Roche) and were denatured by 10 min of boiling in hybridization buffer, and then cooled on ice. The hybridization buffer is the prehybridization buffer supplemented with 100 mg/ml dextran sulfate (Sigma), 100 μg/ml tRNA, 50 μg/ml heparin. Hybridization was performed in a humid chamber with 50% formamide at 55°C by floating the grids on the denatured probe at 0.5–1 μg/ml for 16 hr. The unbound probe was washed off by three washes of prehybridization buffer followed by the IEM labeling protocol described above. The grids were incubated with anti-biotin antibodies followed by protein A gold conjugates. In controls lacking probe, no labeling was visible in the cytoplasm except for some background labeling of sticky yolk granules and mitochondria.

Supplemental Data

Supplemental Data include six figures, one table, and Supplemental Experimental Procedures and are available at http://www.developmentalcell.com/cgi/content/full/13/4/523/DC1/.

ACKNOWLEDGMENTS

We thank the Davis and Rabouille laboratories as well as David Tollervey for helpful discussions, and Robin Allshire, Edele Marston, and Veronique van de Bor for their critical comments on the manuscript. We thank Richard Parton and David Kelly for help and advice with light microscopy, Russell Hamilton and Georgia Vendra for help with statistics, and Carine Meignin for proposing to use an anti-GFP antibody to inhibit SqdGFP. This work was supported by a Wellcome Trust Senior Research fellowship (067413) to I.D., and a Marie Curie fellowship to R.D. B.H. was funded by a Nederlandse Organisatie voor Wetenschappelijk Onderzoek (NWO) Aspasia grant (015.001.129) to C.R.

Received: August 16, 2006
Revised: January 27, 2007
Accepted: August 29, 2007
Published: October 9, 2007

REFERENCES

Anderson, P., and Kedersha, N. (2006). RNA granules. J. Cell Biol. *172*, 803–808.

Bashirullah, A., Halsell, S.R., Cooperstock, R.L., Kloc, M., Karaiskakis, A., Fisher, W.W., Fu, W., Hamilton, J.K., Etkin, L.D., and Lipshitz, H.D. (1999). Joint action of two RNA degradation pathways controls the timing of maternal transcript elimination at the midblastula transition in *Drosophila melanogaster*. EMBO J. *18*, 2610–2620.

Bertrand, E., Chartrand, P., Schaefer, M., Shenoy, S.M., Singer, R.H., and Long, R.M. (1998). Localization of ASH1 mRNA particles in living yeast. Mol. Cell *2*, 437–445.

Bullock, S.L., and Ish-Horowicz, D. (2001). Conserved signals and machinery for RNA transport in *Drosophila* oogenesis and embryogenesis. Nature *414*, 611–616.

Bullock, S.L., Nicol, A., Gross, S.P., and Zicha, D. (2006). Guidance of bidirectional motor complexes by mRNA cargoes through control of dynein number and activity. Curr. Biol. *16*, 1447–1452.

Caceres, L., and Nilson, L.A. (2005). Production of *gurken* in the nurse cells is sufficient for axis determination in the *Drosophila* oocyte. Development *132*, 2345–2353.

Chekulaeva, M., Hentze, M.W., and Ephrussi, A. (2006). Bruno acts as a dual repressor of oskar translation, promoting mRNA oligomerization and formation of silencing particles. Cell *124*, 521–533.

Clark, A., Meignin, C., and Davis, I. (2007). A Dynein-dependent shortcut rapidly delivers axis determination transcripts into the *Drosophila* oocyte. Development *134*, 1955–1965.

Davis, I., Girdham, C.H., and O'Farrell, P.H. (1995). A nuclear GFP that marks nuclei in living *Drosophila* embryos; maternal supply overcomes a delay in the appearance of zygotic fluorescence. Dev. Biol. *170*, 726–729.

Delanoue, R., and Davis, I. (2005). Dynein anchors its mRNA cargo after apical transport in the *Drosophila* blastoderm embryo. Cell *122*, 97–106.

Deshler, J.O., Highett, M.I., and Schnapp, B.J. (1997). Localization of *Xenopus* Vg1 mRNA by Vera protein and the endoplasmic reticulum. Science *276*, 1128–1131.

Forrest, K.M., and Gavis, E.R. (2003). Live imaging of endogenous RNA reveals a diffusion and entrapment mechanism for nanos mRNA localization in *Drosophila*. Curr. Biol. *13*, 1159–1168.

Geng, C., and MacDonald, P.M. (2006). Imp associates with Squid and Hrp48 and contributes to localized expression of *gurken* in the oocyte. Mol. Cell. Biol. *26*, 9508–9516.

Glotzer, J.B., Saffrich, R., Glotzer, M., and Ephrussi, A. (1997). Cytoplasmic flows localize injected oskar RNA in *Drosophila* oocytes. Curr. Biol. *7*, 326–337.

Gonzalez-Reyes, A., Elliott, H., and St Johnston, D. (1995). Polarization of both major body axes in *Drosophila* by Gurken-Torpedo signaling. Nature *375*, 654–658.

Goodrich, J.S., Clouse, K.N., and Schüpbach, T. (2004). Hrb27C, Sqd and Otu cooperatively regulate gurken RNA localization and mediate nurse cell chromosome dispersion in *Drosophila* oogenesis. Development *131*, 1949–1958.

Herpers, B., and Rabouille, C. (2004). mRNA localization and ER-based protein sorting mechanisms dictate the use of transitional endoplasmic reticulum-Golgi units involved in gurken transport in *Drosophila* oocytes. Mol. Biol. Cell *15*, 5306–5317.

Kanai, Y., Dohmae, N., and Hirokawa, N. (2004). Kinesin transports RNA: isolation and characterization of an RNA-transporting granule. Neuron *43*, 513–525.

Kruse, C., Jaedicke, A., Beaudouin, J., Bohl, F., Ferring, D., Guttler, T., Ellenberg, J., and Jansen, R.P. (2002). Ribonucleoprotein-dependent localization of the yeast class V myosin Myo4p. J. Cell Biol. *159*, 971–982.

MacDougall, N., Clark, A., MacDougall, E., and Davis, I. (2003). *Drosophila* gurken (TGFα) mRNA localizes as particles that move within the oocyte in two dynein-dependent steps. Dev. Cell *4*, 307–319.

Malikov, V., Kashina, A., and Rodionov, V. (2004). Cytoplasmic dynein nucleates microtubules to organize them into radial arrays in vivo. Mol. Biol. Cell *15*, 2742–2749.

Navarro, C., Puthalakath, H., Adams, J.M., Strasser, A., and Lehmann, R. (2004). Egalitarian binds dynein light chain to establish oocyte polarity and maintain oocyte fate. Nat. Cell Biol. *6*, 427–435.

Neuman-Silberberg, F.S., and Schüpbach, T. (1993). The *Drosophila* dorsoventral patterning gene *gurken* produces a dorsally localized RNA and encodes a TGF α-like protein. Cell *75*, 165–174.

Norvell, A., Kelley, R.L., Wehr, K., and Schüpbach, T. (1999). Specific isoforms of Squid, a *Drosophila* hnRNP, perform distinct roles in *gurken* localization during oogenesis. Genes Dev. *13*, 864–876.

Norvell, A., Debec, A., Finch, D., Gibson, L., and Thoma, B. (2005). Squid is required for efficient posterior localization of *oskar* mRNA during *Drosophila* oogenesis. Dev. Genes Evol. *215*, 340–349.

Parton, I., and Davis, I. (2005). Time-lapse cinematography in living *Drosophila* tissues. In Live Cell Imaging: A Laboratory Manual, D. Spector and D. Goldman, eds. (Cold Spring Harbor, NY: Cold Spring Harbor Laboratory Press), pp. 385–407.

Parton, I., and Davis, I. (2006). Deconvolution: lifting the fog. In Cell Biology: A Laboratory Handbook, J. Celis, ed. (New York: Academic Press), pp. 187–200.

Pearson, J., and Gonzalez-Reyes, A. (2004). Egalitarian and the case of the missing link. Nat. Cell Biol. *6*, 381–383.

Pfister, K.K., Shah, P.R., Hummerich, H., Russ, A., Cotton, J., Annuar, A.A., King, S.M., and Fisher, E.M. (2006). Genetic analysis of the cytoplasmic dynein subunit families. PLoS Genet *2*, e1.

Roth, S., and Schüpbach, T. (1994). The relationship between ovarian and embryonic dorsoventral patterning in *Drosophila*. Development *120*, 2245–2257.

Saunders, C., and Cohen, R.S. (1999). The role of oocyte transcription, the 5′UTR, and translation repression and derepression in *Drosophila gurken* mRNA and protein localization. Mol. Cell *3*, 43–54.

Schmid, M., Jaedicke, A., Du, T.G., and Jansen, R.P. (2006). Coordination of endoplasmic reticulum and mRNA localization to the yeast bud. Curr. Biol. *16*, 1538–1543.

St Johnston, D. (2005). Moving messages: the intracellular localization of mRNAs. Nat. Rev. Mol. Cell Biol. *6*, 363–375.

Swan, A., and Suter, B. (1996). Role for Bicaudal-D in patterning the *Drosophila* egg chamber in mid-oogenesis. Development *122*, 3577–3586.

Tekotte, H., and Davis, I. (2002). Intracellular mRNA localization: motors move messages. Trends Genet. *18*, 636–642.

Tekotte, H., and Davis, I. (2006). Bruno: a double turn-off for Oskar. Dev. Cell *10*, 280–281.

Van Buskirk, C., and Schüpbach, T. (2002). Half pint regulates alternative splice site selection in *Drosophila*. Dev. Cell *2*, 343–353.

Vorobjev, I., Malikov, V., and Rodionov, V. (2001). Self-organization of a radial microtubule array by dynein-dependent nucleation of microtubules. Proc. Natl. Acad. Sci. USA *98*, 10160–10165.

Weil, T.T., Forrest, K.M., and Gavis, E.R. (2006). Localization of *bicoid* mRNA in late oocytes is maintained by continual active transport. Dev. Cell *11*, 251–262.

Wilkie, G.S., and Davis, I. (2001). *Drosophila wingless* and *pair-rule* transcripts localize apically by dynein-mediated transport of RNA particles. Cell *105*, 209–219.

Wilkie, G.S., Shermoen, A.W., O'Farrell, P.H., and Davis, I. (1999). Transcribed genes are localized according to chromosomal position within polarized *Drosophila* embryonic nuclei. Curr. Biol. *9*, 1263–1266.

Wilsch-Brauninger, M., Schwarz, H., and Nusslein-Volhard, C. (1997). A sponge-like structure involved in the association and transport of maternal products during *Drosophila* oogenesis. J. Cell Biol. *139*, 817–829.